THE JOURNAL OF BIOLOGICAL CHEMISTRY VOL. 283, NO. 49, pp. 34283–34293, December 5, 2008

p66^{Shc}-generated Oxidative Signal Promotes Fat Accumulation*[S]

Received for publication, June 6, 2008, and in revised form, October 1, 2008 Published, JBC Papers in Press, October 6, 2008, DOI 10.1074/jbc.M804362200

Ina Berniakovich[‡§], Mirella Trinei[¶], Massimo Stendardo[‡§], Enrica Migliaccio[‡§], Saverio Minucci[‡¶], Paolo Bernardi[‖], Pier Giuseppe Pelicci[‡§], and Marco Giorgio[‡§1]**

*From the [‡]European Institute of Oncology, Via Ripamonti 435, 20141 Milan, Italy, [§]Firc Institute for Molecular Oncology and [¶]Genextra SpA, Via Adamello 16, 20139 Milan, Italy, [‖]Dipartimento di Scienze Biochimiche, University of Padova, 35128 Padova, Italy, and **Dipartimento di Medicina, Chirurgia e Odontoiatria, University of Milano, 20142 Milan, Italy*

Reactive oxygen species (ROS) and insulin signaling in the adipose tissue are critical determinants of aging and age-associated diseases. It is not clear, however, if they represent independent factors or they are mechanistically linked. We investigated the effects of ROS on insulin signaling using as model system the p66^{Shc}-null mice. p66^{Shc} is a redox enzyme that generates mitochondrial ROS and promotes aging in mammals. We report that insulin activates the redox enzyme activity of p66^{Shc} specifically in adipocytes and that p66^{Shc}-generated ROS regulate insulin signaling through multiple mechanisms, including AKT phosphorylation, Foxo localization, and regulation of selected insulin target genes. Deletion of p66^{Shc} resulted in increased mitochondrial uncoupling and reduced triglyceride accumulation in adipocytes and *in vivo* increased metabolic rate and decreased fat mass and resistance to diet-induced obesity. In addition, p66$^{Shc-/-}$ mice showed impaired thermo-insulation. These findings demonstrate that p66^{Shc}-generated ROS regulate the effect of insulin on the energetic metabolism in mice and suggest that intracellular oxidative stress might accelerate aging by favoring fat deposition and fat-related disorders.

Genetic evidence suggests that insulin/IGF1 signaling in the adipose tissue plays a critical role in the regulation of lifespan in both invertebrates and mammals; (i) overexpression in the fat tissue of Foxo, a key target of insulin/IGF-1 signaling that is inactivated by insulin/IGF-1, prolongs lifespan in *Drosophila* and *Caenorhabditis elegans* (1–3) (ii) fat-specific disruption of the insulin receptor gene decreases body fat and increases lifespan in mice (FIRKO mice) (4, 5). Furthermore, sirtuin1 (SIRT1), the mammalian ortholog of the life-extending yeast gene silent information regulator 2 (SIR2), inhibits adipogenesis of precursor cells and reduces fat storage in differentiated adipocytes by repressing the peroxisome proliferator-activated receptor-γ nuclear receptor, a master regulator of fat cell development in the insulin/IGF1 signaling pathway (6).

At the molecular level evidence suggests that the most important mechanisms of aging involve damage to cellular macromolecules. Reactive oxygen species (ROS)[2], as generated by mitochondria during respiration, induce oxidative stress, which accumulates over life and is considered the proximal mechanism of aging and a major determinant of lifespan (free radical or mitochondrial theory of aging) (7). Indeed, mutations of p66^{Shc}, a gene that increases production of mitochondrial ROS, or overexpression of catalase, which increases their scavenging, prolong lifespan in mice (8, 9). Whether these lifespan determinants (insulin/IGF1 signaling in the fat tissue and oxidative stress) are mechanistically related is unknown.

Recent data showed that one specific ROS molecule, hydrogen peroxide (H_2O_2), is directly implicated in the physiological regulation of different signal transduction pathways, including the insulin/IGF1 pathway (10). Induction of cell proliferation by insulin or IGF1 as well as several other growth factors (*e.g.* epidermal growth factor or platelet-derived growth factor) correlates with a transient increase of intracellular H_2O_2, whereas anti-oxidant treatments prevent insulin/IGF-1-induced DNA synthesis (10, 11). Exogenously added H_2O_2 leads to functional inactivation of tyrosine and serine/threonine phosphatases and activation of tyrosine kinases and various transcription factors (see the following supplemental references: Ross *et al.* (2007), Meng *et al.* (2004), Chiarugi *et al.* (2005). Finkel *et al.* (2000), Paravicini *et al.* (2006)).

The property of H_2O_2 to function as signaling molecule is based on its ability to induce fully reversible protein modifications. It has been demonstrated that H_2O_2 oxidizes directly cysteinyl thiol, inducing disulfide bonds and sulfenic acids formation, and induces glutathionylation of cysteine residues or sulfoxidation of methionine residues in a variety of molecular targets (see the following supplemental references: Song *et al.* (2006), Bossis *et al.* (2006), Davis *et al.* (2000), Ahn *et al.* (2003)). In the case of the PTP1B and PTEN phosphatases, which are directly involved in the attenuation of the insulin/IGF1 signaling, it has been shown that H_2O_2-

* This work was supported, in whole or in part, by National Institutes of Health Grant 1P01AG025532-01A1. This work was also supported by grants from Associazione Italiana per la Ricerca sul Cancro. The costs of publication of this article were defrayed in part by the payment of page charges. This article must therefore be hereby marked "*advertisement*" in accordance with 18 U.S.C. Section 1734 solely to indicate this fact.

[S] The on-line version of this article (available at http://www.jbc.org) contains supplemental references and Figs. 1–4.

[1] To whom correspondence should be addressed: Istituto Europeo di Oncologia Via Ripamonti 435, 20139 Milano, Italy. Tel.: 39-02-94375040; Fax: 39-02-94375990; E-mail: marco.giorgio@ifom-ieo-campus.it.

[2] The abbreviations used are: ROS, reactive oxygen species; MAPK, mitogen-activated protein; BSA, bovine serum albumin; HF, high fat; BAT, brown adipose tissue; FA, fatty acid; H2-DCFDA, 6-carboxy-2′,7′-dichlorodihydrofluorescein (DCF) diacetate; WB, Western blotting; FCCP, carbonyl cyanide-*p*-trifluoromethoxyphenylhydrazone; WT, wild type; siRNA, small interfering RNA; QPCR, quantitative PCR; MOPS, 4-morpholinepropanesulfonic acid; TG, triglyceride; WAT, white adipose tissue.

induced protein modifications are functionally relevant (12, 13). It appears, therefore, that H_2O_2 regulates directly the intensity of insulin/IGF1 signaling within cells.

Indirect evidence suggests that ROS are also involved in the regulation of fat development. Treatment with antioxidants prevents *in vitro* differentiation of pre-adipocytes and, in mice, diet-induced obesity (14). Caloric restriction in laboratory rodents reduces their adipose tissue mass, extends lifespan, and is associated with decreased oxygen metabolism and, consequently, mitochondrial H_2O_2 production (15, 16). It is not clear, however, whether these effects of H_2O_2 or antioxidants on fat development are mediated by modifications of the insulin/IGF1 signaling pathway in the adipose tissue.

A role for ROS as signaling molecules is further supported by recent findings that the generation of H_2O_2 by mitochondria is not just the byproduct of respiration but can also be the result of specific enzymatic systems, such as p66^{Shc}. p66^{Shc} functions as an inducible redox enzyme, which is activated by stress and generates H_2O_2 to trigger apoptosis (17). For this function, p66^{Shc} uses reducing equivalents of the mitochondrial electron transfer chain through the direct oxidation of cytochrome *c* (17). The H_2O_2 generated by p66^{Shc} is ~30% that of the total pool of intracellular H_2O_2 and is biologically relevant, as shown by p66^{Shc} ability *in vitro* and *in vivo* to induce mitochondrial permeability transition and by the findings that cells and tissues derived from p66$^{Shc-/-}$ mice accumulate significantly less oxidative stress (17–25). It is not known, however, whether p66^{Shc}-generated H_2O_2 is also involved in the regulation of receptor-activated signal transduction pathways. We report here that p66^{Shc}-generated H_2O_2 regulates insulin signaling in adipocytes and fat development and propose that the insulin-p66^{Shc} oxidative signaling pathway regulates energetic metabolism.

EXPERIMENTAL PROCEDURES

Reagents—Antibodies against AKT, pAKT, pMAPK, FOXO1, and pFoxo1 were from Cell Signaling; anti-Shc and anti-pShc were from BD Transduction Laboratories and Alexis; anti-PTEN, anti-IRS-1, anti-p85a, and anti-GLUT4 were from Santa Cruz; the anti-phosphotyrosine was from Upstate, and human recombinant insulin was from Roche Applied Science.

Mice—This study was performed according to national law and following authority guidelines. Experiments were carried out on p66$^{Shc-/-}$ and WT mice (Sv/129 and C57Bl/6), maintained in a temperature-controlled room with a 12-h light/12-h dark cycle. A high fat (HF) diet (D12492 with 60% kcal from fat) was purchased from Research Diets Inc. Eight-week-old mice were fed with standard diet or D12492 diet. C57Bl/6 and 129Sv mice were fed HF diet and tap water or water supplemented with 40 mM *N*-acetylcysteine.

Blood glucose levels were measured using Accu-Chek active; triglycerides, cholesterol, and free fatty acid levels were measured using the Reflotron Plus system from Roche Applied Science. Body weight was measured weekly. Total body fat mass was evaluated after chemical extraction as described (26). Measurements of energy expenditure were made using a closed-circuit dual-gas respirometer (Micro-Oxymax System, Columbus Instruments).

Adipocyte Preparation and Treatments—Primary brown pre-adipocytes were isolated from brown adipose tissue (BAT) of intrascapular fat pads from 2-day-old newborns upon digestion with 1.5 mg/ml collagenase type IV buffer (125 mM NaCl, 5 mM KCl, 1.3 mM $CaCl_2$, 5 mM glucose, 100 mM Hepes, 4% BSA) for 40 min at 37 °C. Cells were then plated in growth media (Dulbecco's modified Eagle's medium supplemented with 20% fetal bovine serum, 20 mM HEPES). The following day cultures were washed twice with phosphate-buffered saline, then after confluence, 2×10^5 cells were plated in 12-well dishes in Dulbecco's modified Eagle's medium plus 10% fetal bovine serum. The day after, media were supplemented with insulin at different dosages as indicated and in the presence of 1 nM T3 (27). Lipids accumulation was evaluated after 6 days. Differentiation for some experiments was induced with 40 ng/ml insulin plus 250 μM α-lipoic acid or 0.1 μM antimycin A or 1 μM dexamethasone and 1 mM isobutylmethylxanthine.

Primary white adipocytes were isolated from abdominal white fat pads from 1-month-old mice. Fat pieces were minced and digested with 1.5 mg/ml collagenase type IV at 37 °C for 35 min. Cells were filtered through 250-μm cell strainer, centrifuged at 250 *g*, and plated in the same media as for BAT-derived cells. At day 2 upon confluence, cells were stimulated with 1 μg/ml insulin, and lipid accumulation was evaluated after 10 days with Oil red-O staining.

For retroviral infections, pre-adipocytes were infected on day 2 of culture with empty pBABE vectors or vectors expressing WT p66^{Shc} or the p66^{Shc}*qq* or p66^{Shc}*a* mutants and selected with 2 μg/ml puromycin.

For ROS analysis, levels of intracellular H_2O_2 were determined using 6-carboxy-2′,7′-dichlorodihydrofluorescein (DCF) diacetate (H2-DCFDA). Briefly, cells were treated with 20 μM H2-DCFDA for 45 min in dark (20). Intracellular DCF fluorescence was detected and quantified by fluorescence-activated cell sorter. Direct fluorescence imaging of attached cells stained with H2-DCFDA was also performed to confirm fluorescence-activated cell sorter analysis data. For siRNA down-regulation of p66^{Shc} expression, pre-adipocytes were transfected with a p66^{Shc}-specific 5′-GTACAACCCACTTCGGAATG (28) and a scrambled nucleotide sequence as a negative control, siRNAs.

Biochemistry and Immunofluorescent Analysis—For insulin stimulation experiments cells were serum-starved for 24 h and then treated with 1 μg/ml insulin for 90 min (for FOXO1 and p66^{Shc} activation) or for 5 min (for AKT activation). For immunofluorescence cells were fixed in paraformaldehyde, permeabilized for 10 min with 0.4% Triton X-100 in phosphate-buffered saline supplemented with 0.2% BSA, blocked for 30 min in 2% BSA, and incubated with primary anti-FOXO antibodies produced in rabbit and then with secondary anti-rabbit IgC conjugated with Cy3. For biochemical analysis, cells were washed and lysed in a buffer containing 50 mM HEPES, pH 7.5, 150 mM NaCl, 10% glycerol, 1% Triton X-100, 1.5 mM $MgCl_2$, 1 mM EGTA, 100 mM NaF, 10 mM sodium pyrophosphate, and 500 μM sodium orthovanadate supplemented with a protease inhibitors mixture from Calbiochem. Immunoprecipitations were performed on a platform rocker at 4 °C. Equal amounts of proteins were incu-

bated with anti-Shc or anti-IRS-1 antibodies and then with 50 μl of protein A-agarose followed by 3 washes with lysis buffer. Beads were resuspended in 2× Laemmli loading buffer, and proteins were separated by 8% SDS-PAGE. After SDS-PAGE, proteins were transferred to a polyvinylidene difluoride membrane. The immunoprecipitates were analyzed by Western blotting using indicated antibodies. All blotting steps were performed according to the manufacturer's instructions. Chemiluminescence was detected with ECL Western blotting detection reagent from Amersham Biosciences.

Fatty Acid Intake and Oxidation Rate in Cell Cultures—To determine FA intake and oxidation rate, isolated BAT adipocytes were grown to confluence, washed with phosphate-buffered saline, 0.5% BSA, incubated at 37 °C for 90 min with 1 μCi/ml [^{14}C]oleate (Amersham Biosciences) in Dulbecco's modified Eagle's medium supplemented with 10% fetal bovine serum and 0.5% BSA, washed twice with phosphate-buffered saline, 0.5% BSA, and lysed in 200 μl of 0.5 N NaOH. After neutralization, radioactivity was counted with a liquid scintillation analyzer and normalized for protein content. Fatty acid β-oxidation rate was assessed by the release of $^{14}CO_2$ after [^{14}C]oleate uptake as described (29).

Gene Expression Analysis—Primary BAT pre-adipocytes were grown to confluence and incubated with or without 100 nM insulin for 4 h. Cells then were lysed in a guanidine-isothiocyanate containing buffer, and total RNA was extracted using RNeasy kit (Qiagen) following the manufacturers instructions. For each experiment, total RNA was isolated and pooled from triplicate culture dishes and used for microarrays Affymetrix GeneChip hybridization. Biotin-labeled cRNA targets were obtained from 3 μg of total RNA derived from samples as described above. cDNA synthesis was performed with Invitrogen SuperScript Custom cDNA synthesis kit, and biotin-labeled antisense RNA was transcribed using the *in vitro* MEGAscript High Yield Transcription kit (Ambion Inc., Austin, TX) and included Bio-11-UTP and Bio-11-CTP (PerkinElmer Life Sciences) in the reaction. GeneChip hybridization, washing, staining, and scanning were performed according to Affymetrix (Santa Clara, CA) protocols. A copy of the Mouse Genome 430 2.0 GeneChip Array was hybridized with each target. Absolute and comparative analyses were performed with Affymetrix GeneChip Operating Software (GCOSv1.4), scaling all images to a TGT value of 500. Results were further exported to GeneSpring GX software Version 7.3 (Agilent Technology). For quantitative PCR (QPCR) validation of gene-chip data, total RNA from three independent experiments was reverse-transcribed using Superscript II reverse transcriptase (Invitrogen), and the obtained cDNA was analyzed by quantitative real-time PCR using specific primers for selected genes and Taqman chemistry. Results were expressed as -fold change relative to the controls after normalization using GAPDH gene expression levels.

Bioenergetics—Fresh mitochondria were prepared from mouse BAT using differential centrifugation protocol as described (30). Each mitochondrial preparation (0.5 mg of protein/ml mitochondrial suspension) was assayed (for state 3 determinations, in 100 mM KCl, 50 mM MOPS, 10 mM K_2PO_4, 10 mM $MgCl_2$, 1 mM EGTA, and 0.2% BSA when indicated, pH 7.20) for respiration using a Clark-type oxygen electrode according to standard procedures in the presence of different energetic substrates (5 mM succinate, 1 mM pyruvate/1 mM malate, 10 mM glycerol 3-phosphate) and modulators (0.1 μM dinitrophenol, 5 μM carbonyl cyanide-*p*-trifluoromethoxyphenylhydrazone, 0.4 mM ADP, 0.4 mM GDP, 5 mM palmitate), which were added to glycerol 3-phosphate-energized mitochondria. Mitochondrial transmembrane potential was measured according to the procedure described (31).

Statistical Analysis—Data are presented as the mean ± S.D. and analyzed by Student's *t* test. Differences between means were assessed by one-way analysis of variance. The minimum level of significance was set at $p < 0.05$.

RESULTS

Insulin Activates the Redox Activity of $p66^{Shc}$ in Adipocytes—$p66^{Shc}$ is expressed in primary adipocytes (32) and supplemental Fig. 1*A*) where it is rapidly phosphorylated on Ser-36 after insulin treatment (Fig. 1*A*). After phosphorylation in the cytosol, $p66^{Shc}$ binds to the peptidyl-prolyl isomerase Pin-1 and undergoes a major conformational change that favors translocation of $p66^{Shc}$ within mitochondria and activation of its redox enzymatic activity (33).

Phosphorylation-defective mutants of $p66^{Shc}$ are unable to maintain proper levels of intracellular H_2O_2 and to mediate pro-apoptotic stress signals (17, 33). We investigated whether insulin treatment induces H_2O_2 accumulation in BAT primary pre-adipocytes, as reported for other cell types (34) and whether this effect is mediated by phosphorylation of $p66^{Shc}$. Intracellular levels of H_2O_2 were determined by fluorescence-activated cell sorter analysis of cells stained with H2-DCFDA, a molecular probe that becomes fluorescent upon oxidation by H_2O_2. Steady-state levels of H_2O_2 in $p66^{Shc-/-}$ adipocytes were reduced by ~35% as compared with control WT cells (Fig. 1*B*). Insulin treatment induced a 2–3-fold increase of H_2O_2 in WT BAT pre-adipocytes, whereas it had no effect on $p66^{Shc-/-}$ cells (Fig. 1*C*). Reintroduction of $p66^{Shc}$ but not of the phosphorylation-defective $p66^{Shc}$ Ser36Ala ($p66^{Shc}a$) mutant into $p66^{Shc-/-}$ pre-adipocytes restored insulin-induced H_2O_2 up-regulation (Fig. 1*C*), demonstrating that $p66^{Shc}$ phosphorylation is critical to the ability of insulin to increase intracellular H_2O_2. To demonstrate that $p66^{Shc}$ mediates insulin-dependent H_2O_2 up-regulation through its redox activity, we used the redox-defective mutant $p66^{Shc}$E132Q,E133Q ($p66^{Shc}qq$), which is unable to oxidize cytochrome *c* and to produce mitochondrial ROS (17). Expression of the $p66^{Shc}qq$ mutant in $p66^{Shc-/-}$ BAT pre-adipocytes failed to mediate H_2O_2 up-regulation after insulin stimulation (Fig. 1*C*). Together, these findings demonstrate that insulin activates the redox activity of $p66^{Shc}$ and that $p66^{Shc}$ mediates insulin redox signaling.

$p66^{Shc}$-generated H_2O_2 Regulates Insulin-dependent Activation of AKT-FOXO1 in Adipocytes—Insulin-stimulated H_2O_2 modulates proximal and distal insulin signaling at least in part through the oxidative inhibition of phosphatases that negatively regulate the insulin pathway (PP2A, PTEN) (35).

Tyrosine phosphorylation of IRS-1, the intracellular target of activated insulin-receptor, did not differ significantly in

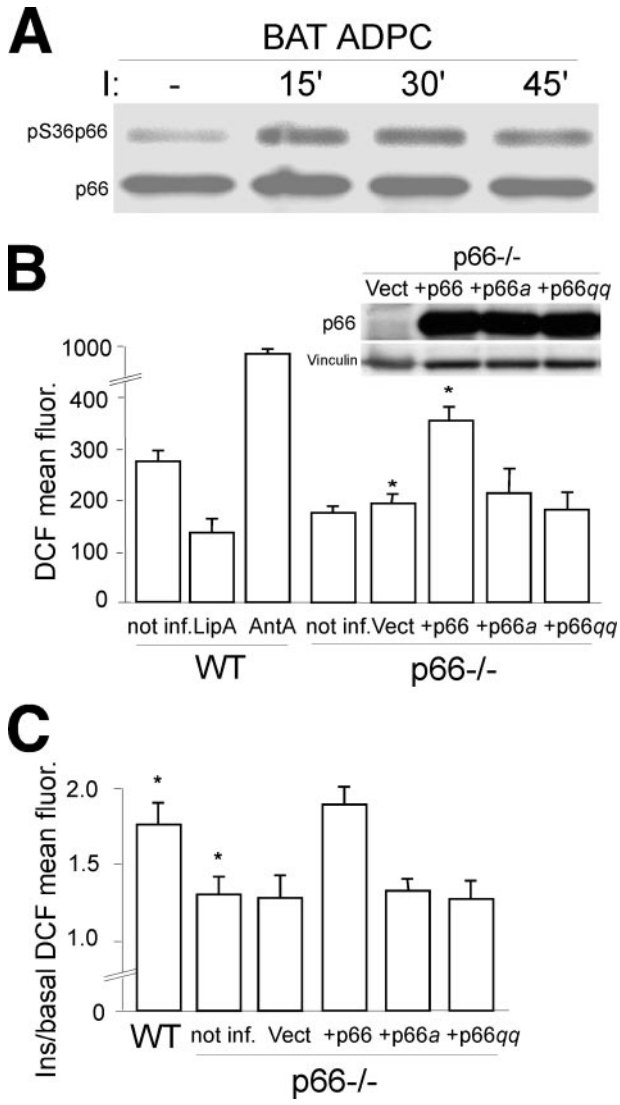

FIGURE 1. **p66^{Shc} redox activity in adipocyte.** *A*, p66^{Shc} Ser-36 phosphorylation before and after insulin treatment (at the indicated time points) of BAT adipocytes (*ADPC*). Anti-Shc immunoprecipitates were analyzed by WB using antibodies against phosphorylated (*upper panel*) or total (*lower panel*) p66^{Shc}. *B*, fluorescence-activated cell sorter analysis of the mean DCF fluorescence of DCFDA-stained WT BAT adipocytes under basal conditions (*not inf.*) or after lipoic acid (*LipA*) or antimycin A (*AntA*) treatment, and p66$^{Shc-/-}$ BAT adipocytes under basal conditions (*not inf.*) or after infection with empty retroviral vector (*Vect*), or retroviral vectors expressing p66^{Shc}, p66^{Shc}*a*, or p66^{Shc}*qq* whose expression levels, as detected by WB in one representative experiment, are shown in the pictures on the *right*. *C*, insulin induced increase of DCF mean fluorescence (ratio between the mean fluorescence of insulin stimulated and untreated cells) in WT BAT adipocytes and p66$^{Shc-/-}$ BAT adipocytes under basal conditions (*not inf.*) or after infection with empty retroviral vector (*Vect*), or retroviral vectors expressing p66^{Shc}, p66^{Shc}*a*, or p66^{Shc}*qq*.

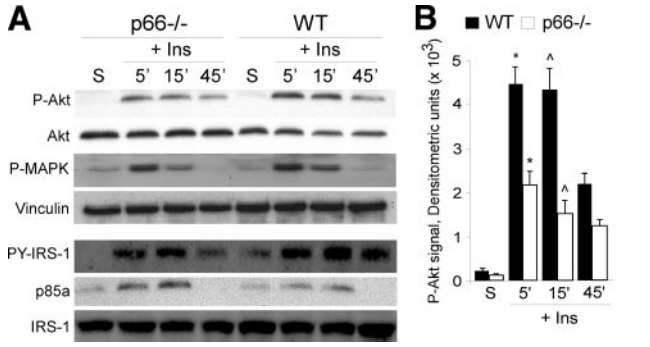

FIGURE 2. **p66^{Shc} regulation of Akt phosphorylation.** *A*, WT and p66$^{Shc-/-}$ BAT adipocytes were starved (*S*) or treated with insulin (*Ins*) and analyzed at the indicated time points. *Top four panels*: WB of total (*Akt*) and phosphorylated (*P-Akt*) AKT, phosphorylated MAPK (*P-MAPK*), and vinculin. *Bottom three panels*: WB of anti-IRS1 immunoprecipitates using antibodies against IRS-1, pY-IRS-1, and p85a. *B*, densitometric analysis of P-Akt signals; the phospho-Akt signal was normalized against total-Akt signal (average values from three independent experiments: * and ^, $p < 0.01$).

the WT and p66$^{Shc-/-}$ samples (Fig. 2*A*; the slight decrease of IRS-1 phosphorylation at later time points after insulin treatment was not seen in other separated experiments). Once phosphorylated, IRS-1 binds various adapter molecules, such as p85 and Grb-2, which activate, respectively, the phosphatidylinositol 3-kinase-AKT and the Ras-MAPK pathways (36). Analysis of the association of IRS-1 with the p85 subunit of phosphatidylinositol 3-kinase in WT and p66$^{Shc-/-}$ BAT pre-adipocytes revealed no differences (Fig. 2*A*). On the contrary, in the p66$^{Shc-/-}$ pre-adipocytes, the extent of insulin-induced AKT phosphorylation was markedly reduced as compared with WT adipocytes, whereas MAPK phosphorylation proceeded normally (Fig. 2, *A* and *B*), indicating that loss of p66^{Shc} affects the phosphatidylinositol 3-kinase-AKT branch in particular.

Among the several targets of activated AKT, the Forkhead transcription factor FOXO1 couples insulin signaling to adipocyte differentiation (37). AKT-dependent FOXO1 phosphorylation leads to its cytoplasmic sequestration and inhibition of transcription from FOXO1-target genes (37). Immunofluorescence analysis of WT BAT pre-adipocytes showed massive relocalization of FOXO1 in the cytoplasm after insulin treatment (from 80 to 5% of cells with nuclear FOXO-1), which was markedly reduced in p66$^{Shc-/-}$ cultures (from 80 to 75%) (Fig. 3, *A* and *B*). It appears, therefore, that p66^{Shc} expression is indispensable for the activation of the AKT-FOXO1 pathway after insulin treatment. Notably, the effect of p66^{Shc} on FOXO1 appeared more pronounced than the effect on AKT, suggesting that p66^{Shc} regulates insulin signaling at multiple levels.

To determine whether the effect of p66^{Shc} on insulin-mediated AKT-FOXO1 activation was dependent on its redox activity, we analyzed the signaling functions of phosphorylation- and redox-defective p66^{Shc} mutants and the effect of p66^{Shc} on oxidation of PTEN, which dephosphorylates and inactivates PIP3, a lipid second messenger produced by phosphatidylinositol 3-kinase (35). Re-expression of WT p66^{Shc} into p66$^{Shc-/-}$ BAT pre-adipocytes restored a normal response of FOXO1 to insulin treatment (from 70 to 5% cells with nuclear FOXO-1), whereas the p66^{Shc}*a* or p66^{Shc}*qq* mutants had no effects (Fig. 3*B* and supplemental Fig. 1*B*). PTEN is inactivated by endogenous H_2O_2 that catalyzes the formation of a disulfide bond between the PTEN active sites Cys-124 and Cys-71. This event correlates with a shift in its electrophoretic mobility in non-reducing PAGE (12). In p66$^{Shc-/-}$ pre-adipocytes, the ratio between reduced PTEN (the slowly migrating form) and oxidized PTEN (the fast migrating form) was increased with respect to the same ratio observed in WT pre-adipocytes both in basal conditions (100% of increase) and after insulin treatment (30% of increase) (Fig. 3*C*, *left panel*), whereas total PTEN levels,

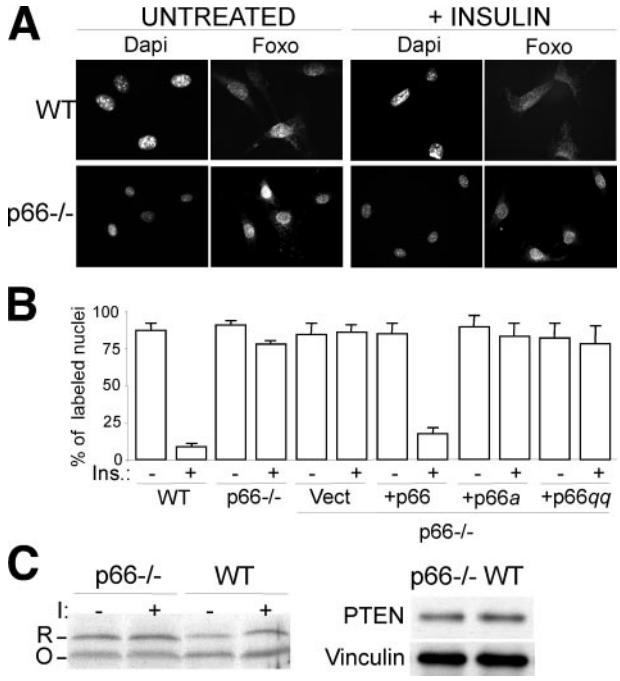

FIGURE 3. **p66^{Shc} regulation of insulin-induced Foxo re-localization.** *A*, 4,6-diamidino-2-phenylindole (*Dapi*) staining of nuclei and immunofluorescence analysis of Foxo1 localization in untreated and insulin-treated WT and p66$^{Shc-/-}$ BAT adipocytes. Images are representative of four experiments which gave comparable results. *B*, percentage of untreated and insulin-treated BAT adipocytes with Foxo1 nuclear localization (results from three experiments). *C*, Western blot analysis using non-reducing PAGE (*left panel*) of reduced (*R*) *versus* oxidized (*O*) forms of PTEN in WT and p66$^{Shc-/-}$ BAT adipocytes before (−) and after (+) insulin (*I*) treatment and using standard reducing SDS-PAGE (*right panel*) of total PTEN in WT and p66$^{Shc-/-}$ BAT adipocytes. Images are representative of four experiments which gave comparable results.

measured by Western blotting (WB) upon reducing SDS-PAGE, was comparable between WT and p66$^{Shc-/-}$ pre-adipocytes (Fig. 3*C*, *right panel*). It appears, therefore, that the ability of p66^{Shc} to regulate FOXO1 activation depends on the integrity of its redox center, suggesting that p66^{Shc} regulates insulin signaling by generating H_2O_2.

p66^{Shc} Regulates Lipogenesis in Adipocytes by Inhibiting Fatty Acid Oxidation—We then investigated the biological contribution of p66^{Shc} to lypogenesis in adipocytes. Because intracellular ROS are critical mediators of insulin-dependent lipogenesis (38), we measured insulin-induced triglyceride (TG) accumulation in WT and p66$^{Shc-/-}$ adipocytes. Treatment of WT BAT (Fig. 4*A*) and white adipose tissue (WAT) (Fig. 4*B*)-derived pre-adipocytes with 40 mg/ml or 1 μg/ml of insulin, respectively, in the presence of 1 nM triiodothyronine (T3) induced TG accumulation in virtually all cells, as seen by Oil red staining 6 and 10 days after treatment (Fig. 4, *A* and *B*). Strikingly, p66$^{Shc-/-}$ adipocytes from both BAT and WAT were almost completely Oil red-negative after the same insulin treatment (Fig. 4, *A* and B). Dose-response analysis of insulin-induced TG accumulation in BAT adipocytes revealed a reduction of insulin sensitivity in the absence of p66^{Shc} expression of about 30-fold (the half-maximal differentiating doses of insulin were 10–20 and 600 ng/ml in WT and p66$^{Shc-/-}$ adipocytes, respectively; Fig. 4*C*). Notably, the effect of p66^{Shc} loss was comparable with that of

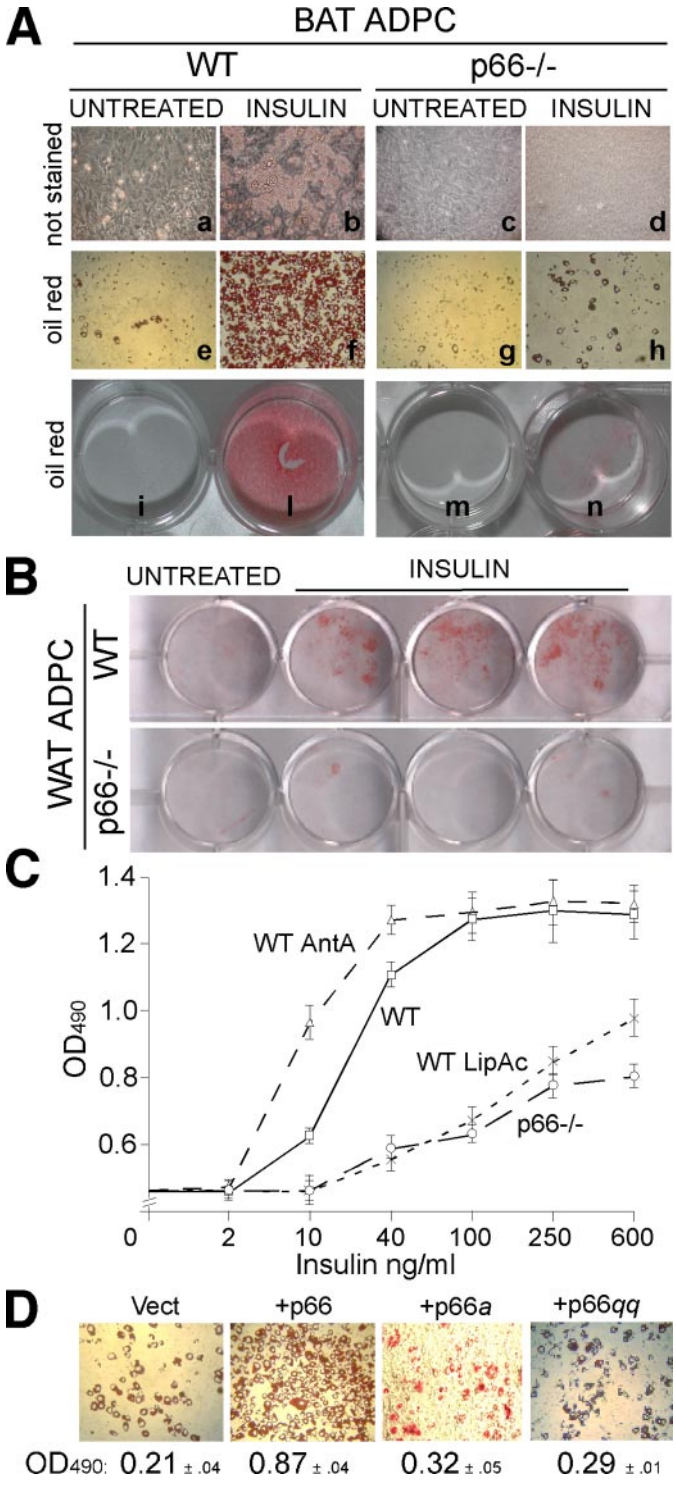

FIGURE 4. **p66^{Shc} regulation of insulin-induced triglyceride accumulation.** *A*, white light microscopy pictures (*a–h*) and plate micrographs (*i–n*) of unstained (*a–d*) and Oil red-stained (*e–h*, *i–n*) BAT adipocytes (*ADPC*) from WT and p66$^{Shc-/-}$ mice. Cells were left untreated (*a*, *e*, *c*, *g*, *i*, and *m*) or treated with insulin for 6 days (*b*, *f*, *d*, *h*, *l*, and *n*). *B*, micrographs of plates of Oil red-stained WT and p66$^{Shc-/-}$ WAT adipocytes (*ADPC*) untreated and after insulin treatment. *C*, optical density (*OD*) values of Oil red extracts from stained WT, antimycin A (*AntA*)-, or lipoic acid (*LipAc*)-treated WT and p66$^{Shc-/-}$ BAT adipocytes (average of eight independent experiments for each condition). *D*, white light microscopy pictures of Oil red-stained p66$^{Shc-/-}$ BAT adipocytes infected with empty (*Vect*), p66^{Shc}, p66^{Shc}*a*, or p66^{Shc}*qq* retroviruses and treated with insulin and their corresponding optical density (*OD*; 490 nm) values.

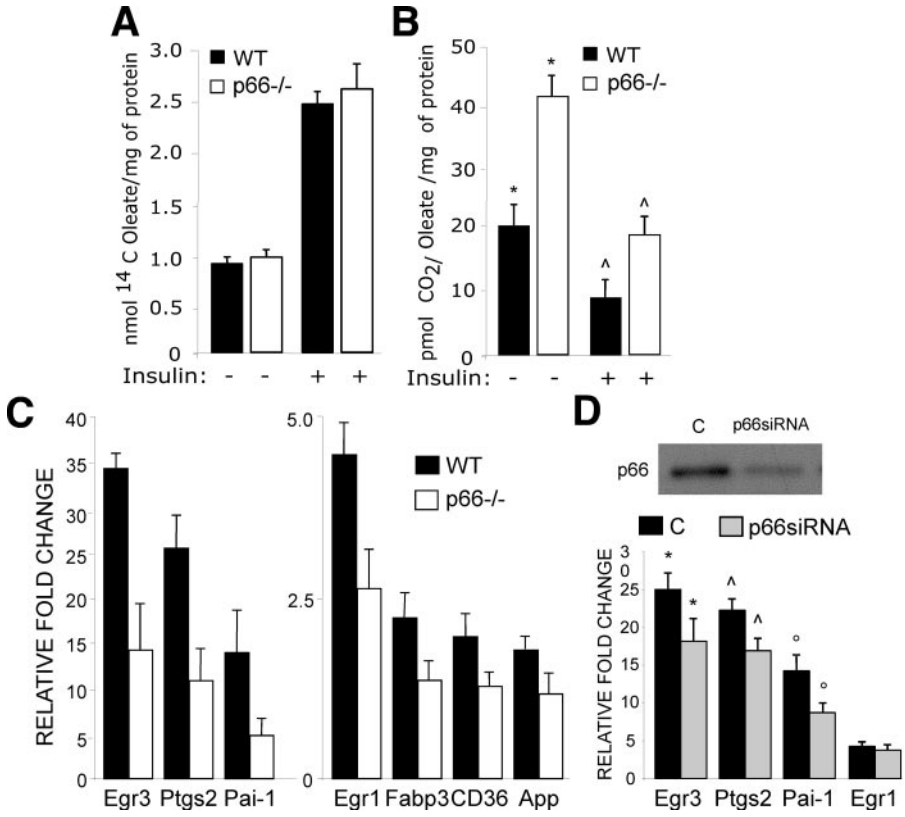

FIGURE 5. **p66^{Shc} regulation of energetic substrate consumption and insulin-dependent gene expression in adipocytes.** *A* and *B*, cells were labeled with [^{14}C]oleate, left untreated, or treated with insulin as indicated. FA uptake and release were measured as ^{14}C incorporation (*A*) and $^{14}CO_2$ release (*B*). *C*, quantitative RT-PCR analysis of transcripts from the indicated genes in WT and p66$^{Shc-/-}$ adipocytes untreated or treated with insulin as indicated. Results are shown as ratio of values from insulin treated *versus* untreated samples. *D*, QPCR analysis of transcripts from the indicated genes in WT adipocytes treated (p66^{Shc}-siRNA) or not (*C*) with siRNA oligos for p66^{Shc} (resulting p66^{Shc} levels are shown in the *upper panel*). Results from three QPCR measurements, each performed on two different siRNA experiments, were reported. *, ^, and °, $p < 0.05$.

antioxidants, such as lipoic acid (Figs. 1*B* and 4*C*) or *N*-acetylcysteine (not shown). Conversely, levels of ROS and insulin-induced lipid accumulation were increased by antimycin A, an inhibitor of respiration that increases mitochondrial ROS generation (Figs. 1*B* and 4*C*). Re-expression of p66^{Shc}, but not of the p66^{Shc}*a* or p66^{Shc}*qq* mutants, in p66$^{Shc-/-}$ BAT pre-adipocytes restored insulin-induced TG accumulation (Fig. 4*D*). Adipocyte differentiation by other stimuli (3-isobutyl-1-methylxanthine and dexamethasone (supplemental Fig. 1*C*) proceeded normally in the p66$^{Shc-/-}$ BAT pre-adipocytes, suggesting that the effect of p66^{Shc} is specific for insulin-induced lipogenesis.

In adipocytes, TG accumulation stimulated by insulin is determined by increased uptake of FA or glucose and inhibition of FA oxidation. To investigate FA metabolism, we measured ^{14}C incorporation (FA uptake) and $^{14}CO_2$ release (FA β-oxidation) in cells preincubated with [^{14}C]oleate. Although the rate of [^{14}C]oleate uptake was similar in basal and insulin-treated WT and p66$^{Shc-/-}$ BAT pre-adipocytes (Fig. 5*A*), the release of $^{14}CO_2$ was higher in p66$^{Shc-/-}$ cells both at the steady state and after insulin treatment (Fig. 5*B*). Together, these results indicate that p66^{Shc} controls the lipogenic function of insulin in adipocytes by inhibiting FA oxidation.

To investigate whether p66^{Shc} regulates selectively downstream adipogenic effectors of the insulin signaling pathway, we performed global gene expression analysis of WT and p66$^{Shc-/-}$ BAT pre-adipocytes treated or not with insulin (4 h). Biotinylated cRNA targets were synthesized from RNA pools of three independent experiments and hybridized to Affymetrix oligonucleotide chips. Analysis of microarray data identified two overlapping lists of 598 and 610 genes regulated by insulin in WT and p66$^{Shc-/-}$ pre-adipocytes, respectively (supplemental Fig. 2).

QPCR validation of 30 gene regulations revealed full concordance (not shown). Cross-comparisons of WT and p66$^{Shc-/-}$ gene sets distinguished three groups of insulin targets; (i) 282 genes regulated by insulin in both WT and p66$^{Shc-/-}$ pre-adipocytes (p66^{Shc}-independent insulin targets); (ii) 316 genes regulated by insulin in WT but not p66$^{Shc-/-}$ pre-adipocytes (p66^{Shc}-dependent targets), and (iii) 328 genes regulated by insulin in p66$^{Shc-/-}$ but not WT pre-adipocytes (p66^{Shc}-repressed insulin targets) (supplemental Fig. 2). Among the 282 p66^{Shc}-independent insulin targets, several genes linked to adipogenesis have been found, some of which are mechanistically implicated in the process of adipogenesis. Notably, the impaired response to insulin in p66$^{Shc-/-}$ BAT pre-adipocytes is accompanied by a lower induction of these adipogenesis-linked genes (Egr1, Egr3, Ptgs2, Pai-1, Fabp3, CD36, App; Fig. 5*C* and supplementary references). QPCR validation of these targets in p66$^{Shc-/-}$ or in WT BAT pre-adipocytes after depletion of p66^{Shc} expression by siRNA is shown in Fig. 5*D*. This correlates with the observation that insulin response is impaired in p66^{Shc}-deficient BAT pre-adipocytes, although we can not draw any conclusion regarding the contribution of the genes considered to the observed phenotype. Expression of peroxisome proliferator-activated receptor-α, ERRα, PGC1, which are critical regulators of adipocyte differentiation, was instead normal in p66$^{Shc-/-}$ cells (not shown). Together, these data indicate that the effect of p66^{Shc} on insulin-dependent gene expression is restricted to specific transcriptional targets, which might explain selectivity of the effect of p66^{Shc} on lipid accumulation.

p66^{Shc} Improves Mitochondrial Coupling in Adipocytes—We then investigated mitochondrial energetic functions in WT and p66$^{Shc-/-}$ BAT mitochondria and tissue. Oxygraph analysis of energized mitochondria (using either pyruvate/malate or glycerol 3-phosphate) and in the presence of fatty acid-free albumin (to sequester free fatty-acids) revealed

similar levels of oxygen consumption in the WT and p66$^{Shc-/-}$ BAT mitochondria (Table 1). In the absence of albumin, instead, p66$^{Shc-/-}$ mitochondria showed higher levels of oxygen consumption (Table 1). Consistently, the addition of palmitate increased respiration more potently in the p66$^{Shc-/-}$ mitochondria (Table 1), suggesting that respiration is higher in the p66$^{Shc-/-}$ mitochondria when fatty acids are available. Because fatty acids stimulate proton backflow to the mitochondrial matrix (uncoupled respiration), we treated BAT mitochondria with the artificial protonophores dinitrophenol or FCCP. Strikingly, dinitrophenol (not shown) or FCCP (Fig. 6*A*) increased respiration of WT but not p66$^{Shc-/-}$ mitochondria (Table 1), suggesting that p66$^{Shc-/-}$ mitochondria are uncoupled. Treatment with the inhibitor of uncoupling proteins GDP, instead, reduced respiration of WT and p66$^{Shc\ -/-}$ BAT mitochondria to equal levels (Table 1). As seen for the isolated BAT mitochondria, minced BAT from p66$^{Shc-/-}$ mice showed increased respiration upon the addition of succinate ($p < 0.01$), which was not further enhanced by treatment with FCCP. Notably, also basal respiration was higher in p66$^{Shc-/-}$ BAT (Fig. 6*A*).

TABLE 1

Respiratory analysis of WT and p66$^{Shc-/-}$ BAT isolated mitochondria

The average values and S.D. of three independent experiments are indicated.

	Isolated MTC			
	+Fat free BSA		w/o fat free BSA	
	WT	p66$^{-/-}$	WT	p66$^{-/-}$
	nmol/ml/mg of protein			
Basal	11.76 ± 2.43	9.14 ± 3.55	6.95 ± 1.86	6.14 ± 0.40
Pyruvate/malate	36.12 ± 5.24	35.10 ± 6.78	52.68 ± 6.13[a]	64.24 ± 5.37[a]
Glycerol 3-phosphate	50.61 ± 5.94	46.82 ± 5.30	70.32 ± 4.51[b]	96.15 ± 7.16[b]
GDP	35.23 ± 6.36	36.51 ± 6.27	39.71 ± 5.18	42.07 ± 4.23
FCCP	102.34 ± 8.12	113.45 ± 9.26	108.22 ± 9.41	104.26 ± 8.51
Palmitate	79.24 ± 8.19[b]	102.11 ± 9.03[b]		
ADP	94.56 ± 8.22	110.07 ± 7.48		

[a] $p < 0.05$.
[b] $p < 0.01$.

To characterize directly coupling efficiency, we measured the protonmotive force of WT and p66$^{Shc-/-}$ BAT mitochondria using the potentiometric tetramethylrhodamine methyl ester (TMRM). Results showed a slight, yet statistically significant, reduction of the membrane potential of p66$^{Shc-/-}$ energized mitochondria (Fig. 6*B*). Treatment with GDP abolished this difference, further supporting our conclusion that p66$^{Shc-/-}$ mitochondria are uncoupled. Together, these findings suggest that the increased oxygen consumption of p66$^{Shc-/-}$ mitochondria is attributable to increased uncoupled state.

Uncoupled respiration in BAT mitochondria is due to expression of the anion-carrier protein UCP1, which mediates a regulated proton-leak across the mitochondrial membranes (39). Inspection of our microarray data showed that UCP1 is up-regulated in p66$^{Shc-/-}$ adipocytes. QPCR analysis confirmed the increased expression of UCP1 mRNA in the p66$^{Shc-/-}$ adipocytes both under basal conditions and after insulin treatment (Fig. 6*C*). Western blotting showed increased levels of the UCP1 protein in BAT adipose tissue of newborn and adult p66$^{Shc-/-}$ mice as compared with WT controls (Fig. 6*D*). These data indicate that p66^{Shc} inhibits basal and insulin-induced UCP1 expression in adipocytes. Thus, high levels of UCP1 might be responsible for the observed uncoupling state of mitochondria in p66$^{Shc-/-}$ adipocytes.

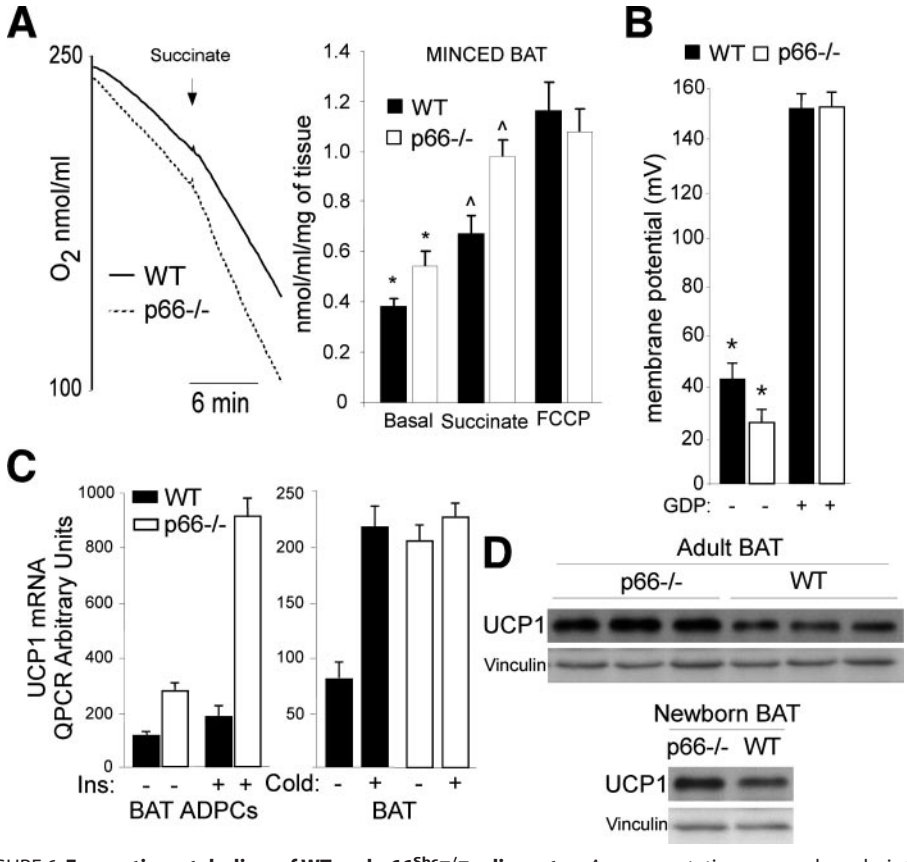

FIGURE 6. **Energetic metabolism of WT and p66$^{Shc-/-}$ adipocytes.** *A*, representative oxygraph analysis (*left panel*) of WT and p66$^{Shc-/-}$-minced BAT tissue. The *graph* on the *right* reports the results from three independent experiments. * and ^, $p < 0.01$. *B*, protonmotive force of WT and p66$^{Shc-/-}$ BAT mitochondria. Results from three independent experiments are reported. *, $p < 0.05$. *C*, quantitative RT-PCR analysis of UCP1 gene expression in WT and p66$^{Shc-/-}$ adipocytes (BAT ADPCs) (untreated or after insulin treatment; *left panel*) and BAT, basal, and cold exposure (*right panel*). *D*, Western blotting analysis of UCP1 protein expression in BAT from adults and newborn WT and p66$^{Shc-/-}$ mice.

p66^{Shc} Induces Fat Development in Vivo—We then investigated the effect of p66^{Shc} on fat accumulation *in vivo*. The body weight of p66$^{Shc-/-}$ mice was normal from birth to 4 weeks of age (not shown). Starting at 2 months of age, p66$^{Shc-/-}$ mice maintained 5–10% lower body weights throughout the rest of their lives as compared

A

	129Sv				C57Bl6			
	Females		Males		Females		Males	
	WT	p66-/-	WT	p66-/-	WT	p66-/-	WT	p66-/-
Total	20.3 ±1.0	18.7 ±1.4	21.1 ±2.0	18.5 ±1.8	22.8 ±2.1	19.4 ±2.0	25.7 ±3.0	22.9 ±1.8
Inguinal^	0.42 ± 0.02	0.30 ± 0.03	0.49 ± 0.05	0.21 ± 0.03	0.50 ± 0.04	0.35 ± 0.04	0.57 ± 0.07	0.26 ± 0.06
Abdominal*	0.55 ± 0.04	0.40 ± 0.04	0.58 ± 0.06	0.24 ± 0.05	0.57 ± 0.10	0.42 ± 0.08	0.71 ± 0.09	0.32 ± 0.06
Scapular°	0.14 ± 0.01	0.10 ± 0.02	0.19 ± 0.01	0.10 ± 0.01	0.16 ± 0.03	0.11 ± 0.03	0.18 ± 0.05	0.09 ± 0.02
Heart	0.20 ± 0.01	0.21 ± 0.01	0.22 ± 0.02	0.23 ± 0.02	0.20 ± 0.02	0.22 ± 0.02	0.22 ± 0.02	0.22 ± 0.04
Brain	0.46 ± 0.02	0.45 ± 0.02	0.46 ± 0.02	0.46 ± 0.03	0.44 ± 0.01	0.44 ± 0.03	0.45 ± 0.03	0.44 ± 0.04

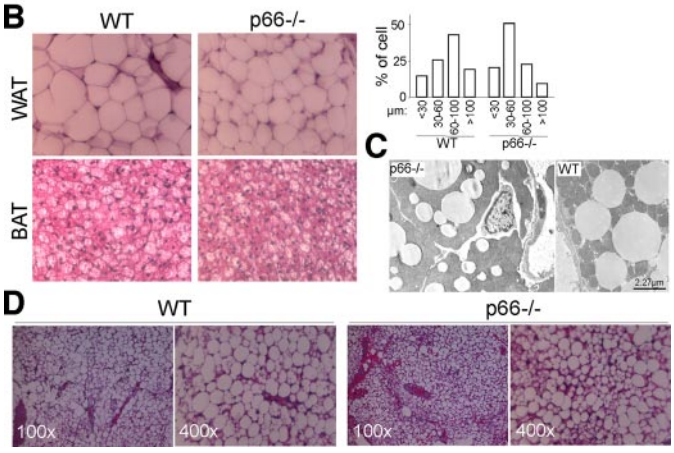

FIGURE 7. **p66^{Shc} regulation of fat accumulation *in vivo*.** *A*, total body (*T*), fat pad (inguinal, abdominal, and scapular), heart (*H*), and brain (*B*) weight in 129Sv or C57Bl6 p66$^{Shc-/-}$ mice (±S.D.; $n = 20$ per group; ^, *, and ° indicates $p < 0.01$ in the comparison of all WT *versus* p66$^{-/-}$ groups in the *row*). *B*, hematoxylin/eosin-staining of WAT and BAT from 8-month-old male mice (*left panel*) and cell size distribution from the same samples (*right panel*). Data represent the result of the analysis of 10 different mice per group. *C*, electron microscopy of WT and p66^{Shc} BAT. *D*, hematoxylin/eosin-staining of WT and p66$^{Shc-/-}$ BAT adipocytes transplants.

with WT mice (Fig. 7*A*) despite normal locomotory activity,[3] food intake (Fig. 8*C*), and overall caloric absorption (as determined by measuring the residual caloric content of feces by calorimetric bomb; not shown). Differences of total body weight between WT and p66$^{Shc-/-}$ mice were mainly due to a ~35% reduction in fat mass in the p66$^{Shc-/-}$ mice (total-body TG content; not shown). Perigonadal, abdominal, and interscapular fat pads were all reduced in p66$^{Shc-/-}$ mice (Fig. 7*A*). Differences were more marked in the abdominal district (75% reduction in the p66$^{Shc-/-}$ males) and were observed in both 129Sv and C57Bl6 p66$^{Shc-/-}$ strains (Fig. 7*A*). No differences between WT and p66$^{Shc-/-}$ mice were observed in the weight of other organs (Fig. 7*A*).

Histological analysis of the same samples showed high cell size heterogeneity, with a larger frequency of adipocytes below 100 μm diameter (Fig. 7*B*). Although the functional significance of this heterogeneity in p66$^{Shc-/-}$ adipose tissue is unclear, it resembles that observed in mice with a null mutation in the insulin receptor gene (FIRKO), which also show reduced fat mass and increased lifespan (5). Electron microscopy examination of BAT (interscapular) in adult p66$^{Shc-/-}$ mice revealed smaller sized lipid deposits in the p66$^{Shc-/-}$ BAT (Fig. 7*C*).

To test whether decreased fat mass in p66$^{Shc-/-}$ mice was due to a cell-autonomous defect of adipocytes, we transplanted WT and p66$^{Shc-/-}$ primary BAT pre-adipocytes into WT nude mice. One month post-transplant, WT adipocytes transplants showed a dramatic increase in size and a decrease in cell heter-

[3] A. Berry and F. Cirulli, manuscript in preparation.

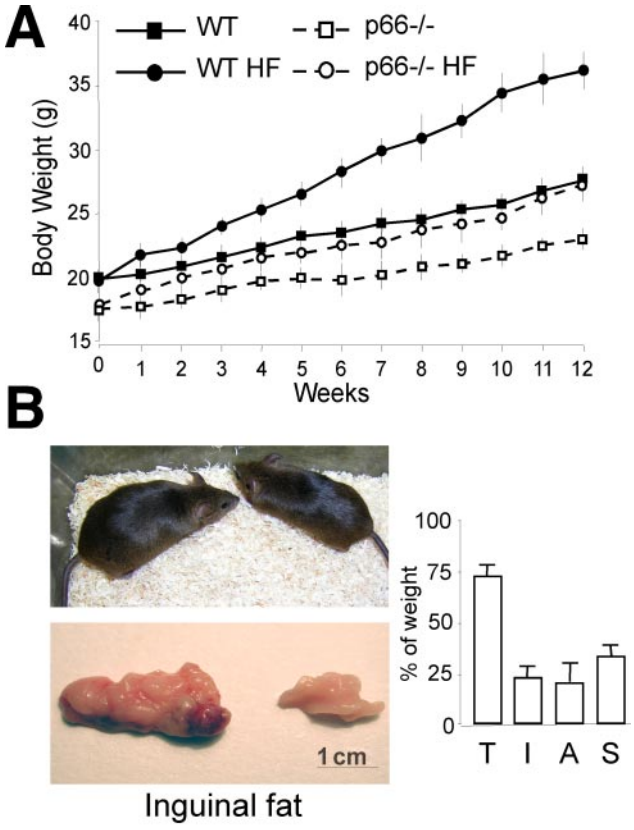

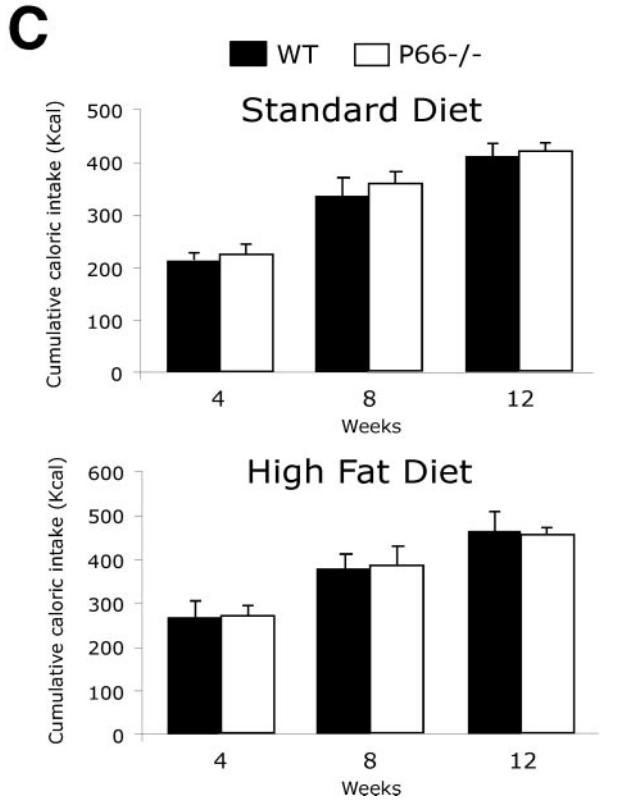

FIGURE 8. **p66$^{Shc-/-}$ prevention of obesity.** *A*, body weight curves of WT and p66$^{Shc-/-}$ male mice fed standard or HF diets. *B*, comparative view of representative p66$^{Shc-/-}$ and WT mice and inguinal fat pads from the same experiment. Total body (*T*) and fat pads (I, inguinal; A, abdominal; S, intrascapular) weight upon HF diet, expressed as in A (*right panel*). *C*, cumulative caloric intake of WT and p66$^{Shc-/-}$ mice at different time points during supplementation with standard (*upper graph*) and high fat (*lower graph*) diets.

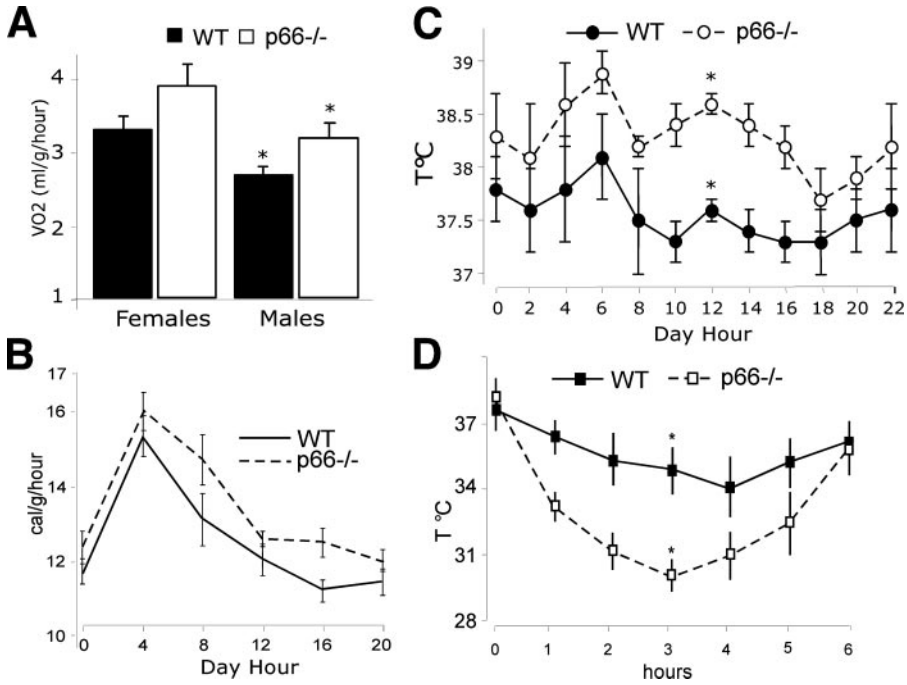

FIGURE 9. **Function of the fat tissue in WT and p66$^{Shc-/-}$ mice.** *A*, O_2 consumption over 24 h of WT and p66$^{Shc-/-}$ mice ($n = 8$ per group); *, $p < 0.01$. *B*, daily energy expenditure of male WT and p66$^{Shc-/-}$ male mice ($n = 8$ per group); *, $p < 0.01$. Shown is the daily body temperature values of WT and p66$^{Shc-/-}$ mice (*C*) and during cold exposure (*D*) ($n = 12$ per group); *, $p < 0.01$.

ogeneity, whereas p66$^{Shc-/-}$ adipocyte transplants grew significantly less, and the cell population remained heterogeneous (Fig. 7*D* and not shown), thus suggesting that reduced fat accumulation in p66$^{Shc-/-}$ mice is the consequence at least in part of an abnormal intrinsic function of adipocytes.

Diet-induced obesity is mediated by insulin-induced lipid accumulation in the fat tissue (5). To determine the role of p66^{Shc} in diet-induced obesity, we studied body weight and fat mass in WT and p66$^{Shc-/-}$ mice fed HF diet for 14 weeks. The profile of circulating lipids after administration of the high fat diet was similar in WT and p66$^{Shc-/-}$ mice (supplemental Fig. 3*A*). As shown in Fig. 8*A*, WT mice gained significantly more body weight than the p66$^{Shc-/-}$ mice (144 *versus* 119% maximal body weight increase, respectively; $p < 0.001$). Notably, the effects of the HF diet on p66$^{Shc-/-}$ mice body weight were comparable with those observed in WT mice supplemented with the anti-oxidant *N*-acetylcysteine in drinking water (supplemental Fig. 3*B* and (40). Gross appearance at sacrifice after 14 weeks of HF diet revealed markedly reduced fat mass in the p66$^{Shc-/-}$ mice as compared with WT animals (Fig. 8*B*). Energetic intake (Fig. 8*C*) and residual fecal caloric content (not shown) were comparable in the two groups. Together these findings demonstrate that p66$^{Shc-/-}$ mice are protected from age-related and diet-induced obesity and suggest that p66^{Shc} is a genetic determinant of fat development in adult mice.

Increased Basal Metabolic Rate and Impaired Cold Adaptation in the p66$^{Shc-/-}$ Mice—We then investigated the functional consequences on energy metabolism of the reduced WAT and BAT in p66$^{Shc-/-}$ mice. WAT is the site where energy is stored after feeding in the form of TG and from where energy is released during periods of fasting in the form of FA. Plasma concentrations of TG, FA, cholesterol, and low density lipoproteins were comparable in WT and p66$^{Shc-/-}$ animals (measured in both the fed and fasted states in age-matched animals of 3, 6, 9, 12, and 18 months; supplemental Fig. 3*A*). Oxygen consumption normalized per body weight was slightly, yet significantly increased in p66$^{Shc-/-}$ males as compared with matched controls (differences did not reach statistical significance in the female animals; Fig. 9*A*). Consistently, energetic expenditure measured in a 24-h interval was moderately higher in the p66$^{Shc-/-}$ male mice (Fig. 9*B*).

WAT has the additional function of protecting from body heat loss (thermo-insulation), whereas BAT generates heat for the maintenance of body temperature when newborn animals are exposed to cold (thermogenesis). The effects of p66^{Shc} loss on thermoregulation were studied by exposing WT and p66$^{Shc-/-}$ mice to cold (5 °C) for 6 h. Basal body temperature was slightly increased in the p66$^{Shc-/-}$ mice (average of 0.6 °C; Fig. 9*C*). The maximal loss of body heat after cold exposure occurred after 4 h in the WT mice and was in the range of 3 °C of body temperature. In the p66$^{Shc-/-}$ mice, instead, maximal loss was around 6 °C and occurred after 3 h (Fig. 9*D*). Notably, both WT and p66$^{Shc-/-}$ mice returned to their basal body temperature after 6 h, suggesting that thermogenesis is not impaired in p66$^{Shc-/-}$ mice (Fig. 9*D*). Thus, abnormal cold adaptation in the p66$^{Shc-/-}$ mice is the consequence of accelerated heat loss, likely due to the reduced thermal insulation effect of fat pads. Notably, levels of UCP1 in p66$^{Shc-/-}$ mice kept at 22 °C were as high as those of WT mice after cold exposure (Fig. 6*C*, *right panel*). All together, these findings suggest that the functional alterations observed in the p66$^{Shc-/-}$ adipocytes translate into critical modifications of the energetic metabolism in p66$^{Shc-/-}$ mice, *e.g.* increased basal body temperature and increased energy expenditure, due to increased BAT metabolism, and accelerated heat loss, due to reduced WAT mass.

DISCUSSION

ROS are implicated in the physiological regulation of the insulin/IGF1 signal-transduction pathway and in the regulation of fat development (10, 11, 14). It is not known, however, whether regulation of fat development by ROS occurs through a direct effect on the insulin/IGF1signaling pathway in the adipose tissue. We reported here that insulin activates the redox enzyme-activity of p66^{Shc} in adipocytes and that p66^{Shc}-generated H_2O_2, through its effect on the insulin-signaling cascade, reduces mitochondrial oxygen consumption and favors TG accumulation. *In vivo*, mice lacking p66^{Shc} showed increased basal metabolism, reduced fat development, and increased

insulin sensitivity of peripheral tissues. We propose that this newly identified insulin-p66^{Shc}-H_2O_2 signaling pathway is a critical determinant of energetic metabolism in mammals.

Our findings demonstrate that p66^{Shc} is a downstream target of the insulin signaling pathway and a critical mediator of insulin-dependent ROS-up-regulation in adipocytes. Furthermore, we showed that phosphorylation- and redox-defective mutants of p66^{Shc} are unable to restore redox signaling by insulin, demonstrating that p66^{Shc} phosphorylation and p66^{Shc} redox activity are both integral to insulin signaling. Based on previous characterization of these two mutants (17), we propose a model whereby insulin stimulation induces phosphorylation of p66^{Shc} in the cytosol, its translocation into the mitochondrial intermembrane space, activation of its redox enzymatic activity, and generation of H_2O_2 (supplemental Fig. 4).

p66^{Shc}-generated H_2O_2 appears to regulate insulin signaling selectively and at multiple levels. In p66$^{Shc-/-}$ adipocytes, activation of AKT by insulin is attenuated, whereas MAPK activation is normal. Selective activation of AKT by p66^{Shc} might be due to a direct effect of p66^{Shc}-generated H_2O_2 on phosphatases that regulate phosphatidylinositol 3-kinase, such as PTEN (35). In this respect we noticed that the effect of p66^{Shc} is much more marked on FOXO, a critical transcription factor downstream of AKT (37), than on AKT itself and that the effect of p66^{Shc} on insulin-dependent gene expression is markedly selective. Some of the gene regulations induced by insulin in WT adipocytes were maintained in the absence of p66^{Shc}; others were attenuated or lost, and "new" transcriptional effects of insulin became evident. Thus, the selective effects of p66^{Shc} on the cellular responses to insulin might be achieved through multiple redox-dependent mechanisms that selectively regulate insulin signaling, including AKT phosphorylation, Foxo1 localization, and selected insulin target genes.

Regulation of insulin signaling by p66^{Shc} results into critical modifications of energy metabolism in adipocytes. By studying the effect of p66^{Shc} deletion in BAT adipocytes, we discovered two functions of p66^{Shc}; they are inhibition of insulin-induced FA oxidation and inhibition of basal and insulin-induced UCP1 expression. These activities of p66^{Shc} led, respectively, to increased TG accumulation in WAT and BAT adipocytes and reduced oxygen consumption in BAT adipocytes, thus contributing to switch the energetic balance of adipocytes toward energy conservation.

One implication of these findings is that p66^{Shc} functions to connect mitochondrial respiration to insulin signaling. Because the mitochondrial electron transfer chain is the source of reducing equivalents for the generation of H_2O_2 by p66^{Shc}, accumulation of energetic substrates in mitochondria is critical for the redox activity of p66^{Shc}. On the other hand, p66^{Shc}-generated H_2O_2 sets the threshold of cellular sensitivity to specific insulin effects, including inhibition of mitochondrial FA consumption and increase of TG accumulation. In this model p66^{Shc} functions as a specific signal transducer that integrates in adipocytes insulin signaling and the mitochondrial energetic state (supplemental Fig. 4). Notably, the consequences of p66^{Shc}-generated redox signals are not equivalent to generic oxidative damage. In fact, ROS are expected to increase lipid peroxidation in mitochondria and, accordingly, decrease mitochondrial coupling (41). p66^{Shc}, instead, generates specifically H_2O_2 but has no effect on other oxygen radicals such as O_2. p66^{Shc}-generated H_2O_2 has marginal effects on mitochondrial lipid peroxidation (not shown) and, on the contrary, signals to increase mitochondrial coupling.

The signaling activity of p66^{Shc} in adipocytes has important *in vivo* consequences. We demonstrated that p66$^{Shc-/-}$ mice have reduced body weight due to reduced mass of both WAT and BAT. In addition, p66$^{Shc-/-}$ mice are protected from diet-induced obesity, suggesting that p66^{Shc} is a genetic determinant of fat development in adult mice. Leanness of the p66$^{Shc-/-}$ mice is not explained by changes in food intake, intestinal absorption of nutrients, or locomotor activity. Rather, it may reflect defective lipogenesis in adipocytes, as suggested by the reduced lipid accumulation of p66$^{Shc-/-}$ adipocytes transplanted into WT recipient mice. This interpretation of the mechanisms leading to decreased fat mass in the p66$^{Shc-/-}$ mice, however, poses the question of how the energy balance is maintained in the absence of p66^{Shc} and why energy storage is reduced. Notably, p66$^{Shc-/-}$ mice showed increased basal body temperature and increased basal metabolic rate, suggesting that the increased uncoupled respiration in the BAT mitochondria of p66$^{Shc-/-}$ mice leads to increased energy expenditure, thus contributing to resistance to body weight gain.

The findings of reduced adiposity in p66$^{Shc-/-}$ mice might have important implications for the effect of p66^{Shc} on lifespan. In conclusion, our findings demonstrate that p66^{Shc}-generated oxidative signal directly regulates the threshold of sensitivity to insulin in adipocytes and the development of fat tissue *in vivo*, suggesting that regulated generation of H_2O_2 has evolved to control energy conservation. Attenuation of p66^{Shc} or insulin signaling in the fat tissue, as by genetic mutations, reduces adiposity and increases lifespan, posing the question of why the threshold of insulin sensitivity is apparently "so low" in the fat tissue under physiological conditions. One could hypothesize that the physiological size of the fat tissue is set to serve other functions, which are evolutionarily more critical than longevity. Adaptation to cold, which is altered in the lean p66$^{Shc-/-}$ mice, could be one of such functions or, alternatively, optimization of energy storage when food is available.

Acknowledgments—We thank Elena Beltrami, Lucilla Titta, and Carlo Tacchetti for many helpful discussions and experimental advices.

REFERENCES

1. Clancy, D. J., Gems, D., Harshman, L. G., Oldham, S., Stocker, H., Hafen, E., Leevers, S. J., and Partridge, L. (2001) *Science* **292,** 104–106
2. Giannakou, M. E., Goss, M., Junger, M. A., Hafen, E., Leevers, S. J., and Partridge, L. (2004) *Science* **305,** 361
3. Hwangbo, D. S., Gershman, B., Tu, M. P., Palmer, M., and Tatar, M. (2004) *Nature* **429,** 562–566
4. Bluher, M., Kahn, B. B., and Kahn, C. R. (2003) *Science* **299,** 572–574
5. Bluher, M., Michael, M. D., Peroni, O. D., Ueki, K., Carter, N., Kahn, B. B., and Kahn, C. R. (2002) *Dev. Cell* **3,** 25–38
6. Guarente, L., and Picard, F. (2005) *Cell* **120,** 473–482
7. Harman, D. (1998) *Ann. N. Y. Acad. Sci.* **854,** 1–7
8. Migliaccio, E., Giorgio, M., Mele, S., Pelicci, G., Reboldi, P., Pandolfi, P. P., Lanfrancone, L., and Pelicci, P. G. (1999) *Nature* **402,** 309–313

9. Schriner, S. E., Linford, N. J., Martin, G. M., Treuting, P., Ogburn, C. E., Emond, M., Coskun, P. E., Ladiges, W., Wolf, N., Van Remmen, H., Wallace, D. C., and Rabinovitch, P. S. (2005) *Science* **308,** 1909–1911
10. Stone, J. R., and Yang, S. (2006) *Antioxid. Redox Signal.* **8,** 243–270
11. Finkel, T. (2000) *FEBS Lett.* **476,** 52–54
12. Lee, S. R., Yang, K. S., Kwon, J., Lee, C., Jeong, W., and Rhee, S. G. (2002) *J. Biol. Chem.* **277,** 20336–20342
13. Yu, C. X., Li, S., and Whorton, A. R. (2005) *Mol. Pharmacol.* **68,** 847–854
14. Cho, K. J., Moon, H. E., Moini, H., Packer, L., Yoon, D. Y., and Chung, A. S. (2003) *J. Biol. Chem.* **278,** 34823–34833
15. Gredilla, R., Lopez-Torres, M., and Barja, G. (2002) *Microsc. Res. Tech.* **59,** 273–277
16. Weindruch, R. (1988) *The Retardation of Aging and Disease by Dietary Restriction*, Charles C. Thomas, Spingfield, IL
17. Giorgio, M., Migliaccio, E., Orsini, F., Paolucci, D., Moroni, M., Contursi, C., Pelliccia, G., Luzi, L., Minucci, S., Marcaccio, M., Pinton, P., Rizzuto, R., Bernardi, P., Paolucci, F., and Pelicci, P. G. (2005) *Cell* **122,** 221–233
18. Khanday, F. A., Yamamori, T., Mattagajasingh, I., Zhang, Z., Bugayenko, A., Naqvi, A., Santhanam, L., Nabi, N., Kasuno, K., Day, B. W., and Irani, K. (2006) *Mol. Biol. Cell* **17,** 122–129
19. Nemoto, S., and Finkel, T. (2002) *Science* **295,** 2450–2452
20. Trinei, M., Giorgio, M., Cicalese, A., Barozzi, S., Ventura, A., Migliaccio, E., Milia, E., Padura, I. M., Raker, V. A., Maccarana, M., Petronilli, V., Minucci, S., Bernardi, P., Lanfrancone, L., and Pelicci, P. G. (2002) *Oncogene* **21,** 3872–3878
21. Zaccagnini, G., Martelli, F., Fasanaro, P., Magenta, A., Gaetano, C., Di Carlo, A., Biglioli, P., Giorgio, M., Martin-Padura, I., Pelicci, P. G., and Capogrossi, M. C. (2004) *Circulation* **109,** 2917–2923
22. Pacini, S., Pellegrini, M., Migliaccio, E., Patrussi, L., Ulivieri, C., Ventura, A., Carraro, F., Naldini, A., Lanfrancone, L., Pelicci, P., and Baldari, C. T. (2004) *Mol. Cell. Biol.* **24,** 1747–1757
23. Napoli, C., Martin-Padura, I., de Nigris, F., Giorgio, M., Mansueto, G., Somma, P., Condorelli, M., Sica, G., De Rosa, G., and Pelicci, P. (2003) *Proc. Natl. Acad. Sci. U. S. A.* **100,** 2112–2116
24. Menini, S., Amadio, L., Oddi, G., Ricci, C., Pesce, C., Pugliese, F., Giorgio, M., Migliaccio, E., Pelicci, P., Iacobini, C., and Pugliese, G. (2006) *Diabetes* **55,** 1642–1650
25. Francia, P., delli Gatti, C., Bachschmid, M., Martin-Padura, I., Savoia, C., Migliaccio, E., Pelicci, P. G., Schiavoni, M., Luscher, T. F., Volpe, M., and Cosentino, F. (2004) *Circulation* **110,** 2889–2895
26. Sjogren, K., Hellberg, N., Bohlooly, Y. M., Savendahl, L., Johansson, M. S., Berglindh, T., Bosaeus, I., and Ohlsson, C. (2001) *J. Nutr.* **131,** 2963–2966
27. Champigny, O., Holloway, B. R., and Ricquier, D. (1992) *Mol. Cell. Endocrinol.* **86,** 73–82
28. Nemoto, S., Combs, C. A., French, S., Ahn, B. H., Fergusson, M. M., Balaban, R. S., and Finkel, T. (2006) *J. Biol. Chem.* **281,** 10555–10560
29. Muoio, D. M., Seefeld, K., Witters, L. A., and Coleman, R. A. (1999) *Biochem. J.* **338,** 783–791
30. Shabalina, I. G., Jacobsson, A., Cannon, B., and Nedergaard, J. (2004) *J. Biol. Chem.* **279,** 38236–38248
31. Scaduto, R. C., Jr., and Grotyohann, L. W. (1999) *Biophys. J.* **76,** 469–477
32. Kao, A. W., Waters, S. B., Okada, S., and Pessin, J. E. (1997) *Endocrinology* **138,** 2474–2480
33. Pinton, P., Rimessi, A., Marchi, S., Orsini, F., Migliaccio, E., Giorgio, M., Contursi, C., Minucci, S., Mantovani, F., Wieckowski, M. R., Del Sal, G., Pelicci, P. G., and Rizzuto, R. (2007) *Science* **315,** 659–663
34. Mahadev, K., Wu, X., Zilbering, A., Zhu, L., Lawrence, J. T., and Goldstein, B. J. (2001) *J. Biol. Chem.* **276,** 48662–48669
35. Tang, X., Powelka, A. M., Soriano, N. A., Czech, M. P., and Guilherme, A. (2005) *J. Biol. Chem.* **280,** 22523–22529
36. Bevan, P. (2001) *J. Cell Sci.* **114,** 1429–1430
37. Nakae, J., Kitamura, T., Kitamura, Y., Biggs, W. H., III, Arden, K. C., and Accili, D. (2003) *Dev. Cell* **4,** 119–129
38. May, J. M., and de Haen, C. (1979) *J. Biol. Chem.* **254,** 9017–9021
39. Rousset, S., Alves-Guerra, M. C., Mozo, J., Miroux, B., Cassard-Doulcier, A. M., Bouillaud, F., and Ricquier, D. (2004) *Diabetes* **53,** S130–135
40. Kim, J. R., Ryu, H. H., Chung, H. J., Lee, J. H., Kim, S. W., Kwun, W. H., Baek, S. H., and Kim, J. H. (2006) *Exp. Mol. Med.* **38,** 162–172
41. Brand, M. D., Affourtit, C., Esteves, T. C., Green, K., Lambert, A. J., Miwa, S., Pakay, J. L., and Parker, N. (2004) *Free Radic. Biol. Med.* **37,** 755–767